Journal of Atmospheric and Solar-Terrestrial Physics 73 (2011) 1117–1128

Contents lists available at ScienceDirect

Journal of Atmospheric and Solar-Terrestrial Physics

journal homepage: www.elsevier.com/locate/jastp

Prominence 3D reconstruction in the STEREO era: A review

A. Bemporad *

INAF-Turin Astronomical Observatory, via Osservatorio 20, 10025 Pino Torinese (TO), Italy

ARTICLE INFO

Article history:
Received 12 March 2010
Received in revised form
7 December 2010
Accepted 7 December 2010
Available online 17 December 2010

Keywords:
Sun: prominences
Sun: UV radiation
Technique: 3D reconstruction

ABSTRACT

Since the launch of the STEREO mission (October 2006) the determination of the real prominence shapes and trajectories during eruptions in three dimensions (3D) became easily viable, thanks to the stereoscopic observations, available for the first time, acquired by the twin STEREO spacecraft. These data give us now a unique capability to identify twisted or ribbon-like structures, helical or planar motions, and to investigate the existence of a real critical height for prominence eruptions without projection effects. All these parameters are of fundamental importance for understanding the physical phenomena triggering the eruption and affecting their early evolution. Many different techniques have been developed and employed after the beginning of the "STEREO era", but important information on the 3D structure of prominences was also derived before STEREO. Hence, the present paper is aimed at reviewing different reconstruction techniques developed both before and after the availability of stereoscopic observations and discusses the advancement made so far on these issues thanks to the pre- and post-STEREO data.

1. Introduction: study of solar prominences

Solar prominences (called filaments, when observed on-disk—Fig. 1) are cool and dense structures, with plasma electron temperatures around $5\times10^3-1.5\times10^5$ K and electron densities of $1.3\times10^9-3\times10^{11}$ cm^{-3} (Patsourakos and Vial, 2002). The filament plasma is denser and cooler than the surrounding coronal plasmas which are invisible in images in relatively cool lines such as Hα and He II λ304; filaments are usually observed as dark structures against the chromosphere because they scatter light from the chromosphere and photosphere. They are also observable against the solar background in the extreme ultraviolet (EUV) lines if the background is sufficiently bright that they scatter light at these wavelengths also. However, during episodes called "activations", filament threads or whole sections of filaments are occasionally seen in emission in various EUV lines as well as in Hα, indicating the occurrence of plasma heating (Labrosse et al., 2010; Mackay et al., 2010). Prominences are believed to be kept in equilibrium by the surrounding magnetic field, and many different models have been proposed so far to understand the prominence formation, mass supply, stability and to explain their instabilities leading to prominence eruptions and coronal mass ejections (CMEs). Nevertheless, the final solutions to these problems have not been found so far (see Patsourakos and Vial, 2002 for a comprehensive review on the prominence science from SOHO data, Labrosse et al., 2010 and Mackay et al., 2010 for two more recent reviews on quiescent prominences). In particular, because of close association with the occurrence of flares and CMEs, understanding the processes involved in filament eruptions continues to be an active area of research (see, e.g. Tonooka et al., 2000; Schmieder et al., 2004; Sterling et al., 2007). Recent solar missions such as STEREO, but also HINODE and SDO, improved our capabilities to perform multi-spacecraft studies of prominence eruptions (see, e.g. Bemporad et al., 2009; Landi et al., 2010).

It is well known that erupting filaments generally exhibit helical structures (e.g. Athay et al., 1983; Rust and Kumar, 1984) and the handedness and full 3D velocity vector of many untwisting CME helixes have been derived from spectroscopic observations acquired by the SOHO *UV Coronagraph Spectrometer* (UVCS; see review by Kohl et al., 2006 and references therein). For this reason a very important quantity often used to characterize the degree of instability of filaments is the magnetic helicity H (Berger and Field, 1984), defined as $H=\int_V \mathbf{B}\cdot\mathbf{A}\,dV$, where V is the volume where H is measured, $\mathbf{B}$ is the magnetic field and $\mathbf{A}=\nabla\times\mathbf{B}$ is the vector potential. The magnetic helicity mainly quantifies how much a set of magnetic flux tubes are sheared and/or wound around each other and can be written as the sum of "twist" and "writhe": the twist measures how much the field lines wind about the magnetic axis of the rope, whereas the writhe quantifies the helical deformation of the axis itself (see Fig. 2, left panels). It has been shown that an important condition for the formation and maintenance of a filament is a "handedness" property known as chirality, which requires the filaments to be either of two types: dextral or sinistral (see review by Martin, 1998 and references therein). The chirality χ of a filament is defined by the sense of rotation (twist) of the magnetic field in reversing from upward pointing on the positive

* Tel.: +39 0 11 8101954.
E-mail address: bemporad@oato.inaf.it

1364-6826/$ - see front matter © 2010 Elsevier Ltd. All rights reserved.
doi:10.1016/j.jastp.2010.12.007

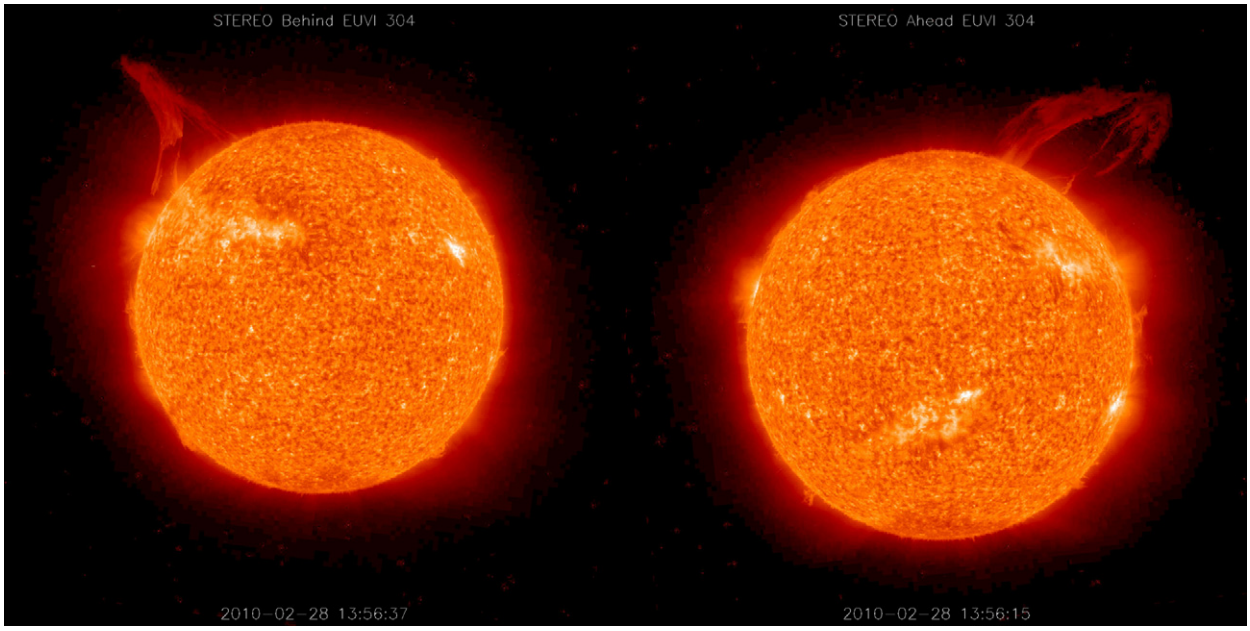

Fig. 1. A huge prominence eruption recently observed by the twin EUVI telescopes onboard STEREO-B (left) and STEREO-A (right) spacecraft. These observations have been acquired with the He II 304 Å filter (corresponding to a plasma temperature around $\sim 8 \times 10^4$ K) on February 28, 2010, when the angle between the STEREO spacecraft was 137.0°).

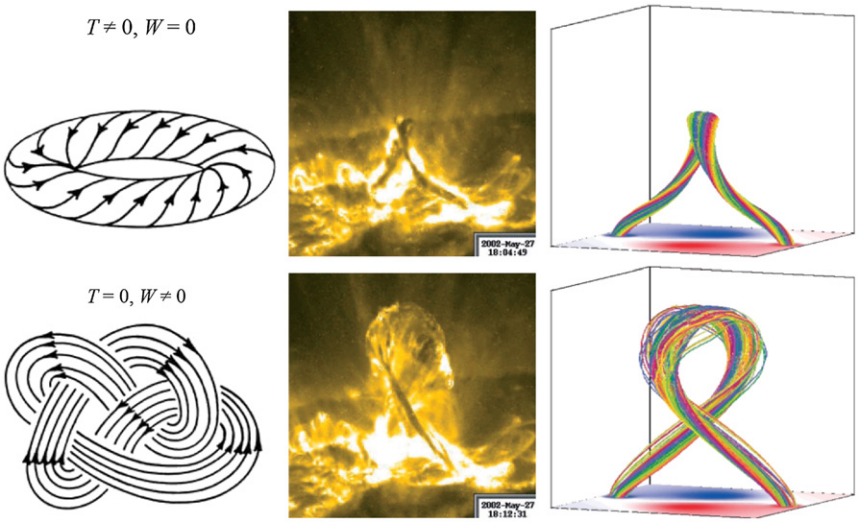

Fig. 2. Left panels: cartoon showing an example of possible magnetic field configurations, where the contribution to the total helicity is separately due only to the twist T (top) or to the writhe W (bottom) of field lines (adapted from Ricca, 1994). Middle and right panels: the confined filament eruption on 2002 May 27 observed by TRACE, and magnetic field lines of the kink-unstable flux rope in the simulation by Török and Kliem (2005); the flux rope axis at the state shown in the bottom frame of the simulation has a writhe of $W = 0.67$.

side of the polarity reversal boundary to downward pointing on the negative side (see, e.g. Martin, 2003); H is a quantitative, mathematical measure of χ.

Helicity H is believed to play a very important role not only in the filament formation, but also in the filament destabilization. For instance, evidence of the existence of a previously unrecognized form of dynamic chirality (handedness) called the "roll effect" has been found in erupting prominences (Martin, 2003). Also, the so-called "helical kink" instability of a magnetic flux rope (see Fig. 2, middle and right panels) is expected to occur when the twist exceeds a critical value (Hood and Priest, 1981). In a high magnetic Reynold number plasma (i.e. in ideal MHD) H is a conserved quantity (even taking into account the effects of magnetic reconnection; Berger and Field, 1984) and the erupting filaments, different from stable filaments, exhibit large scale twist or writhe, clearly appearing as helical-like patterns and rotations during their eruptions. Hence, it is generally believed that prominence eruptions and resulting CMEs are the most efficient way the Sun has to globally "carry out" the excess of helicity built in its interiors by the solar dynamo. The observed rotation of the erupting filament is generally interpreted as a conversion of twist into writhe in a kink-unstable magnetic flux rope (see, e.g. Zhou et al., 2006). Moreover, the conservation of the helicity between filament and the interplanetary *counterpart* of CMEs (ICMEs) is used to associate filament eruptions and magnetic clouds: statistically, the direction of the axial field and helicity of ICMEs (also related to their geoeffectiveness) are consistent with those of the erupted filaments (e.g. Yurchyshyn et al., 2001, 2005).

Despite the efforts devoted in the last decades by the solar community to the problems of formation and stability of solar prominences, many fundamental questions remain unsolved. In particular, many of the still open problems on these phenomena are strictly related to our poor knowledge of the real three-dimensional (3D) structure of these features: for instance, prominences appear different when observed in Hα or in UV, so what is their exact size? Also, what is their fine structure and its impact on their large scale stability or instability? Why do filaments often appear to have a ribbon-like structure and how is this related to the little understood 3D topology of their surrounding magnetic fields? What is the evolution of real (i.e. without projection effects) prominence heights before and during their eruption? Is there a "critical height" (e.g. Filippov and Den, 2001) that indicates an impending eruption and concurrent flare? What is the role played by the magnetic helicity accumulation in the filament stabilization or destabilization? Is the observed rotation of the erupting filaments really a signature of conversion of twist into writhe? Stereoscopic measurements aimed at providing a determination of the real 3D structure and evolution of solar prominences are needed in order to solve the above open problems.

2. The STEREO mission

The *Solar TErrestrial RElations Observatory* (STEREO; see Kaiser et al., 2008) has been mainly designed to observe for the first time with twin instrumentation the Sun from two different viewing angles, thus allowing reconstruction of the real 3D structure of solar phenomena without any limitation due to projection effects. On board the STEREO spacecraft, the *Sun Earth Connection Coronal and Heliospheric Investigation* (SECCHI; see Howard et al., 2008) imaging package includes the EUV imagers (EUVI), the COR1 (inner) and COR2 (outer) coronagraphs and the HI1 (inner) and HI2 (outer) Heliospheric Imagers. The EUVI, COR1-2 and HI1-2 telescopes allow, respectively, studies of prominence/filaments, CMEs and ICMEs. Since the beginning of the STEREO mission (October 25, 2006) huge efforts have been dedicated to the reduction of coronagraphic CME images acquired by the COR1, COR2 telescopes and the HI1 and HI2 Heliospheric Imagers. The aim of these works has been to solve well-known problems related to the line-of-sight integration through the optically thin plasma and to determine the real 3D structure of CMEs. To this end, many different techniques for the 3D reconstruction of CMEs/ICMEs have been developed (see Mierla et al., 2009; Vourlidas and Thernisien, this issue, for reviews) and results from these analyses are now providing very important constraints to be compared with what we already learned in the past decades about the 3D structure of ICMEs from *in situ* measurements in the interplanetary space (see Wimmer-Schweingruber, 2006; Zurbuchen and Richardson, 2006, for reviews).

Observations of the lower corona and chromosphere acquired by EUVI telescopes have been primarily used to infer the 3D shape of coronal loops (Feng et al., 2007) and polar plumes (Curdt et al., 2008), but also to study the 3D structure and kinematic properties of quiescent and erupting prominences/filaments. In particular, the EUVI telescope (Wuelser et al., 2004) has four channels which, similarly to those of SOHO/EIT, have peak responses around 304 Å ($\simeq 8\times10^4$ K, primarily the He II line), 171 Å ($\simeq 1\times10^6$ K, primarily Fe IX/X), 195 Å ($\simeq 1.4\times10^6$ K, primarily Fe XII), and 284 Å ($\simeq 2.2\times10^6$ K, primarily Fe XV). The aim of the present paper is to review the main results obtained so far on the 3D reconstruction of prominences and filaments from the analysis of data acquired by the twin EUVI telescopes onboard STEREO (Fig. 1). STEREO offers substantially increased potential for addressing the classical open questions on solar filaments/prominences because of its two identical EUVI telescopes when they are positioned to see the same features from two different perspectives, along with a third perspective from both ground-based or satellite experiments at Lagrangian point L1 or in orbit around the Earth.

Stereoscopic data acquired by STEREO allow today real 3D stereoscopic reconstructions without strong assumptions. Results from these analyses can be used to answer the open questions listed in the previous section and also to test several predictions of the unified solar eruption model (see, e.g. Forbes, 2000), which relates flares, filament eruptions, and CMEs. In order to help the reader to better understand the impact of the STEREO results, this paper also briefly reviews the main techniques developed prior to the availability of STEREO data to derive important information on the 3D structure of prominences. After comparing the results obtained before and after the STEREO launch, this paper will conclude that, in spite of the increased spatial and temporal resolutions of EUVI telescopes, to date the analyses of STEREO data has not yet significantly improved upon our knowledge of the 3D configuration of filaments in their pre-eruptive and eruptive states. After a short description on present limitations in our understanding of prominence emission in He II line (Section 3), early 3D reconstruction of prominences obtained before the STEREO mission are summarized (Section 4). Then, main results obtained from the analysis of STEREO EUVI data are described (Section 5) and their impact on present understanding are discussed (Section 6).

3. Prominence He II emission

As mentioned above, observations acquired by the EUVI telescopes are available with four different EUV filters: one filter centered on the emission from an He ion (He^{1+}) and three filters centered on the emission from Fe ions (Fe^{8+}, Fe^{11+}, Fe^{14+}). Because of typically low prominence plasma temperatures, these structures are primarily observed in the He filter, hardly visible in the higher temperature Fe filters, where usually a fainter emission is observed at prominence locations (referred as prominence "cavities"). For this reason, 3D reconstructions of filaments and prominences with STEREO data have been performed so far only from images acquired in the He filter. Hence, before describing the main results obtained so far, it is important to review here the main theoretical difficulties in the interpretation of the observed He emission. The limit of the data dealing with imaging observations in the He II λ303.78 line is the complexity in the physical interpretation of the measured fluxes. First, without any information on the observed line profile, it is impossible to discriminate when the measured fluxes are solely due to He II λ303.78 line or also to other spectral lines being integrated in the same filter spectral band, such as the Si XI λ303.32, whose contribution function $G(T)$ (phot cm^{-3} s^{-1} sr^{-1}) peaks at a plasma temperature around $10^{6.2}$ K and is larger than the He II $G(T)$ in a temperature interval between $\sim 1-5\times10^6$ K. Secondly, even when information on the line profiles are available, interpretation of the observed line intensities are difficult because the prominence plasma is optically thick at these wavelengths. Moreover, when the plasma is moving (as in the case of erupting prominences) the diagnostic is even more complex because Doppler dimming occurs.

Comprehensive non-LTE models of He I and He II emissions in a quiescent and an erupting prominence have been recently developed by Labrosse and Gouttebroze (2001) and Labrosse et al. (2007), respectively. These models are complex in that they require to solve the statistical equilibrium and radiative transfer equations in the non-static case by using velocity-dependent boundary conditions for the solution of the radiative transfer problem. By approximating the prominence as a plane-parallel slab standing vertically above the solar surface (Fig. 3, left panel), these authors showed that in a quiescent prominence the He II λ304 line is formed

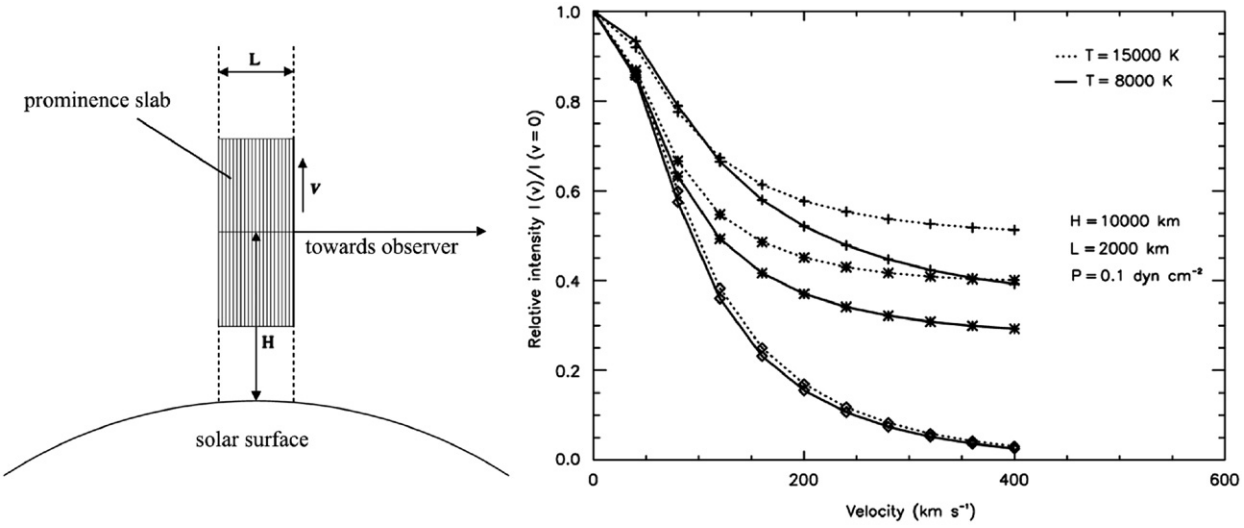

Fig. 3. Left: schematic drawing of the EUV-prominence model designed by Labrosse et al. (2007); the model assumes that the prominence can be described as a plane-parallel slab with thickness L along the line-of-sight, centered at the altitude H above the limb and expanding with velocity **v**. Right: relative integrated prominence intensities as a function of velocity **v** at 8×10^3 K (solid) and 1.5×10^4 K (dots) for He I λ 584 (plus symbols) and 537 Å (asterisks) and He II λ 304 (diamonds; adapted from Labrosse et al., 2007).

mostly by the scattering of the incident radiation, and that for prominences erupting with velocities larger than 150 km s^{-1} there is a strong sensitivity of the observed He II λ304 emission to the plasma expansion velocity (Fig. 3, right panel). As a consequence, the He II λ304 observed emission changes can be primarily ascribed to variations of the prominence expansion velocity rather than variations of other parameters such as the plasma temperature or the prominence thickness. Interestingly, as suggested by the authors, this implies that a measure of Doppler dimming in the resonance He lines can be used to estimate the radial velocity component and, in combination with projected velocity components as observed by SOHO, STEREO and HINODE, to infer the full velocity vector.

Nevertheless, because of the difficulties described above, imaging He II λ304 observations of prominences are quite often employed only to derive kinematical information on the plasma motions, while quantitative estimates on plasma physical parameters are much more complex. In the following sections, I summarize the results obtained for the 3D reconstructions of prominences before the availability of STEREO data, while results obtained from STEREO are described in Section 5 and discussed in Section 6.

4. Prominence 3D reconstructions from non-STEREO data

Before STEREO mission, many attempts have been performed to make use of images acquired by a single ground- or space-based observatory to perform 3D reconstructions of solar structures. Different techniques have been developed such as (in a scattered order) prominence spectroscopic models, multi-slit spectroscopic observations, rotation stereoscopy, geometrical de-projection of two-dimensional (2D) images. These techniques allow to determine important information on the 3D structure of both quiescent and eruptive prominences. This section is aimed at quickly reviewing all these techniques.

4.1. Quiescent prominences

Aschwanden and Bastian (1994) first demonstrated that combinations of solar radio maps obtained by the same observatory on different days can be used to measure the 3D position of radio sources. The idea is to take advantage of solar rotation and to assume that the observed sources were mainly stable with time during the observational period: this method is called rotation stereoscopy. This idea has been applied to estimate the altitude of active region sources at microwave frequencies (Aschwanden et al., 1995) and then the same principle has been developed to determine the altitude above the solar surface of different structures, and in particular of filaments and prominences. Obviously, filament altitudes can be easily determined when the material is dragged by solar rotation to the limb, becoming observable as a prominence, but these observations can be performed only over a few days, making it difficult to study in details the formation and evolution of filaments and eventually their eruptions. But, before the advent of STEREO mission, it was possible to determine the filament heights even when the material was on-disk, from the filament rotation rate observed in full-disk Hα images (see Roša et al., 1998; Vršnak et al., 1999). In particular, these works took advantage of the observed synodic rotation rate of filaments, used as tracers of solar rotation, which becomes apparently larger than the real rotation rate of the filament photospheric footpoint, because of projection effects. A solution is found by treating the height of the filament and the rotation rate of its footpoint as free parameters and by fitting the observed changes of the measured synodic rotation rate during its disk passage. Moreover, an attempt to take into account also the projected filament widths and measure the altitude of the upper edge of the filament has been performed. The same technique has also been applied recently by Brajša et al. (2009) to model prominences and coronal condensations. Nevertheless, these works were based on the assumption that the height of the tracer does not change during the disk passage. They provided only a rough estimate of the tracer altitude as a byproduct of the rotation rate determination. Hence, no information on the evolution of the filament altitude or its 3D structure could be provided.

A complex technique to derive information on the 3D structure of filaments has been proposed by Schwartz et al. (2004, 2006). These techniques used a modified version of the spectroscopic model first developed by Heinzel et al. (2003) to estimate the lower and upper boundaries of the EUV-filament extension along the line-of-sight and radial directions. This model was originally proposed to explain the larger filament extension observed in EUV spectral lines with respect to their Hα counterparts (Heinzel et al., 2001), a difference interpreted as an effect of the much larger optical thickness of the Hydrogen Lyman continuum with respect

to that of Hα. In particular, Schwartz et al. (2004) derived 2D altitude maps for the upper and lower boundaries of a filament observed both in EUV (by SOHO/CDS and SUMER) and Hα for several values of the Hydrogen Lyman continuum optical thickness (Fig. 4). Interestingly, the authors found that the EUV-filament extensions were located at greater altitudes, supporting the idea of a vertically extended twisted flux tube in which the filament plasma is located in shallow magnetic dips. The model also allows estimation of the total mass of the filament, a quantity which plays an important role in the case of filament eruptions (see, e.g. Low et al., 2003, and references therein). Further, Schwartz et al. (2006) modelled the H Lyman line observed profiles, and concluded that the EUV-filament extension is inhomogeneous, with both optically thin and thick areas. Nevertheless, this method is based on many assumptions, viz. the filament is approximated with a very simplified plane-parallel structure, the definition of the EUV-filament extension is uncertain and in some cases there are many points inside the EUV-filament area, where the model gives no results.

4.2. Eruptive prominences

The work described in the previous section deals with stable prominences/filaments. For erupting filaments, information on the 3D motion of blobs and knots can be derived from the observed Doppler shifts of Hα profiles: one of the first efforts tackling this problem dates back to McMath and Pettit (1939). Further efforts in this direction have been made by Martin et al. (1974), who detected Doppler shifts related to plasma motions along the line-of-sight (LOS) occurring in a filament one day before a flare using a multi-slit Hα spectrograph. With a similar instrument, Srivastava and Mathew (1999) were able to measure at the same time the velocity of plasma motions occurring along the LOS (from line Doppler shifts) and on the plane of the sky (POS) in a surge prominence, which allowed the authors to measure the projection angle of the surge in the POS. The technique of 2D Hα spectroscopy was also employed by Mein and Mein (1991) to perform a statistical study of Doppler velocities and line widths in a quiescent prominence, numerically simulated by assuming the existence of many identical unresolved "threads" moving with different velocities with a Gaussian distribution.

An interesting technique to reconstruct the 3D trajectories of erupting prominence blobs has been recently developed by Zapiór and Rudawy (2007). In particular, the authors performed a numerical 3D trajectory reconstruction by analyzing Hα images and spectra acquired by a ground-based Multi-Channel Subtractive Double Pass spectrometer of the Astronomical Institute of the Wroclaw University (see also Rudawy et al., 2003). By comparing plane of the sky-projected velocities with true radial velocities of blobs, as derived from the observed Hα emission images and profiles, it is possible to infer the 3D velocity vector at each instant, which can then be used to reconstruct the 3D trajectories of blobs. Resulting trajectories (Fig. 5) have strong inclinations with respect to the radial direction, implying strong tangential accelerations. More recently, a similar technique has been applied by Schmieder et al. (2010) to study fine scale motions in a quiescent prominence. In this work Hα Dopplergrams obtained with the MSDP instrument in the Meudon Observatory (Paris) have been combined with Hα images provided by the Solar Optical Telescope (SOT) onboard the Hinode satellite. The authors measured the LOS and POS velocity components for many Hα threads within the prominence and found that both components are approximately of the same order (5–15 km s^{-1}). This led the authors to conclude that the quiescent prominence observed by SOT appears as a 2D vertical shape because of the integration along the LOS across quasi-horizontal magnetic field lines in a 3D perspective.

Further, a "prominence height measurement algorithm" was developed by Joshi and Srivastava (2007) to study six erupting quiescent prominences partially located on disk using SOHO/EIT He II λ304. The aim of this work was to de-project the 2D images provided by a single spacecraft and derive 3D information on the observed prominences. To this end, the authors assumed that (a) prominences are linear structures, (b) their footpoints lie on the Sun's surface, and (c) prominences rise normal to the Sun's surface. With these assumptions the authors concluded that the pre-eruption slow rise phase occurs with a small acceleration by 4–12 cm s^{-2}, in contrast to previous studies which suggested that slow rising motions occurs at constant velocity. The slow rise phase was followed by the eruptive phase (where the acceleration is much larger, 10–80 m s^{-2}), that the authors were able to follow from EIT images up to $\sim 2\ R_{\odot}$, demonstrating that the core of the CME corresponds to the prominence observed in He II λ304 images.

Additionally, by following the evolution and shape of filaments, it is also possible to deduce which structures are in front or back of other structures (with respect to the observer) providing a better understanding of the 3D dynamics of filaments during eruption from 2D images. For example, some erupting prominences appear as kinked loops in 2D, while, by knowing the footpoint locations prior to eruption, one can correctly interpret such dynamic

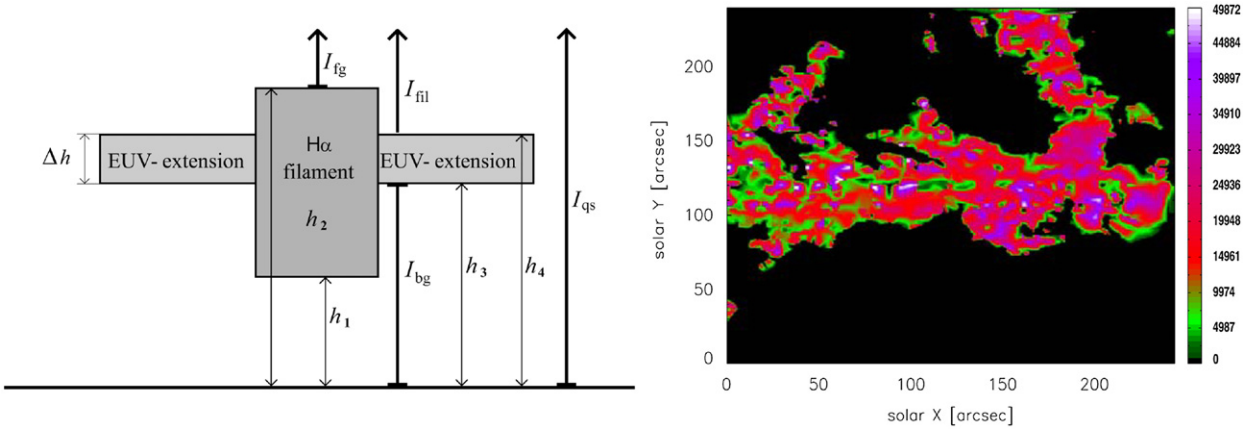

Fig. 4. Left: schematic drawing of the EUV-filament model designed by Heinzel et al. (2003), defining the altitudes of the bottom and top parts of the Hα (h_1 and h_2, respectively) and EUV (h_3 and h_4, respectively) filament extensions (adapted from Schwartz et al., 2004). In the model I_{fg} is the intensity measured at the darkest points within the Hα filament and I_{fil} is the EUV-filament intensity, dependent on the modelled intensity of background radiation incident at the bottom surface of the EUV-filament I_{bg}. Right: an example of a filament altitude map (in particular for the altitude h_3 shown in the left panel) derived by Schwartz et al. (2004).

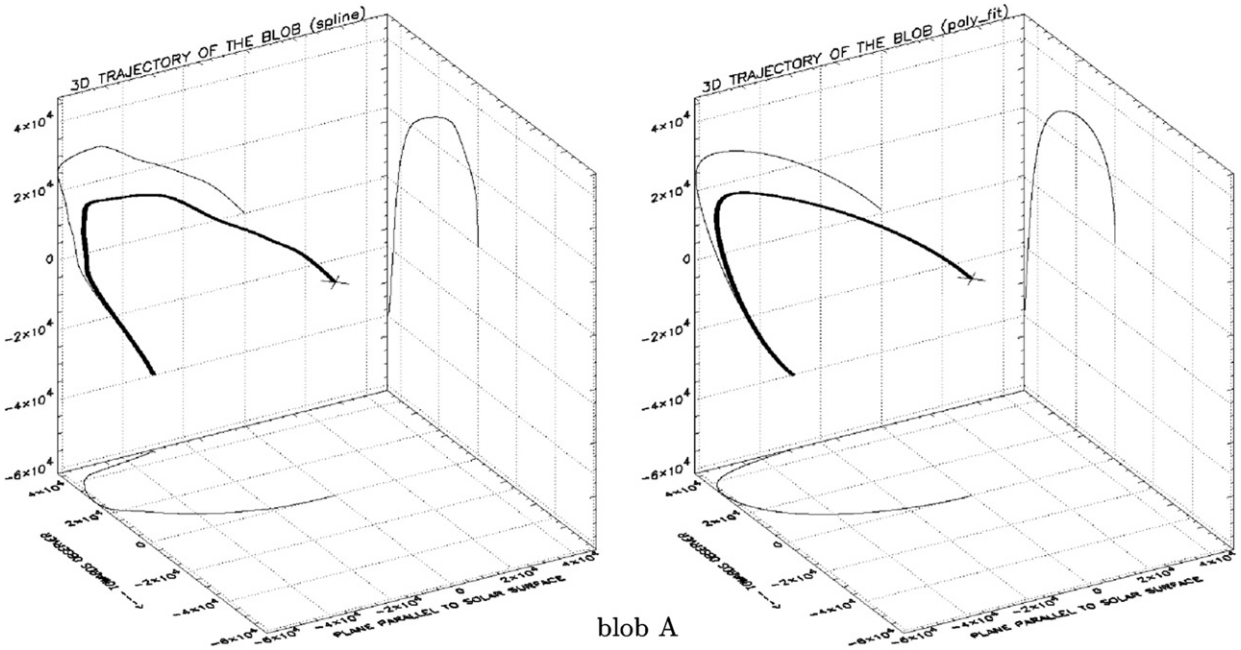

Fig. 5. An example of true 3D trajectory of a blob identified within an erupting prominence with spectrographic Hα images acquired by the MSDP instrument and analyzed with numerical interpolation (left) and polynomial fitting (right) (adapted from Zapiör and Rudawy, 2007.

structures as exhibiting apparent rotation about a vertical axis, as shown in the paper by Green et al. (2007).

Unique information on the rotation of erupting prominences embedded in CMEs has been derived in the last ~ 12 years from the analysis of UVCS data. Spectroscopic observations of CMEs provided for the first time both the plasma velocity components along the LOS (thanks to the line Doppler shifts) and in the radial direction (thanks to the Doppler dimming/pumping effect, see Noci et al., 1987). The first eruption observed by UVCS provided evidence for the rotation of the velocity vector associated with helical motions of plasma around an erupted magnetic flux tube (Antonucci et al., 1997). The line intensity morphologies and line profile Doppler shifts have been used to infer the handedness of untwisting left-handed (Ciaravella et al., 2000) and right-handed (Suleiman et al., 2005) CME helixes and to verify that their handedness was in agreement with that of the pre-CME structures. The variations in the Doppler line shift observed in a CME in the H I Lyman-α line led Ciaravella et al. (2003) to conclude that the leading edge was not an hemispherical shell, but a loop- or ribbon-like structure. Nevertheless, the interpretation of spectroscopic CME data is often ambiguous because the effects of different physical phenomena (e.g. variations of plasma kinetic temperatures, densities and bulk velocities integrated along the LOS) can be mixed.

5. Prominence 3D reconstructions from STEREO data

There are a few works published so far on the 3D reconstruction of prominences from STEREO data; in the following, main results derived from these works are described. In the conclusions (Section 6) these results are summarized and advancement made with respect to the "pre-STEREO era" are discussed.

The first work on this subject (Gissot et al., 2008) deals with the reconstruction of altitude maps for an erupting filament observed by EUVI telescope with the He II λ 304 filter at different times. This work makes use of an "optical flow" algorithm originally developed by Gissot et al. (2003) to estimate from the apparent motion of coronal features observed in two successive SOHO/EIT frames the differential rotation velocity, and later successfully applied also on TRACE images (Gissot and Hochedez, 2007). Gissot et al. (2008) applied their algorithm to first derive from pairs of EUVI He II λ304 images acquired at the same time displacement maps of a filament, i.e. maps of the estimated apparent displacement of different filament parts due to the different viewing angles in the two STEREO-A and -B images. From these displacements maps, derived at a sub-pixel precision, and given the separation angle between the two spacecrafts, an estimate of the filament altitude above the photosphere can be derived pixel by pixel in the EUVI image; resulting altitude maps are shown in Fig. 6. From these maps the authors concluded that the filament started to rise and erupt before the occurrence of the associated B9.2 flare. The authors also concluded that "the eruption occurs without ribbons and post-flare loops because there is no plasma heating in the reconnection site of the erupting filament".

In other works information on the 3D plasma distribution within filaments/prominences have been derived with the so-called "tie-pointing" technique (Bemporad, 2009; Gosain et al., 2009; Liewer et al., 2009; Li et al., 2010). With this method the same feature (as He II knots, ribbons, etc…) is first identified in both images, then the 3D coordinates of the feature are reconstructed by triangulation (Thompson, 2006). This technique makes use of the epipolar geometry: the points P_A and P_B (corresponding to projected apparent positions in 2D STEREO-A and -B images of the same point P) and the point P itself (corresponding to the real position of the observed object) lie on the epipolar plane, defined for any object point P. Given these three points and the separation angle between the spacecrafts, by assuming that the epipolar planes can be considered all parallel to the ecliptic for any point P, epipolar geometry gives the 3D coordinates of P (see Inhester, 2006, for details on the epipolar geometry). If this technique is applied to "many" points P within a chromospheric or coronal feature (e.g. a filament/prominence, a coronal loops, a plume, etc…) information on the 3D distribution and expansion of plasma can be derived. To this end, works cited above made use of the software tools for

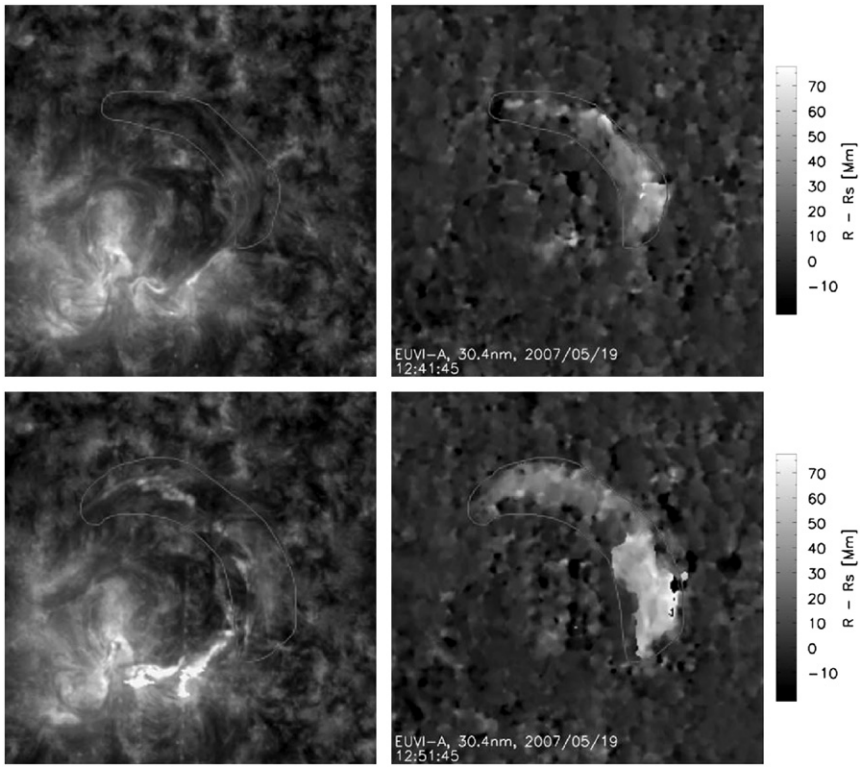

Fig. 6. Left: a zoom on the original EUVI-A He II λ304 images acquired at 12:41 (top) and 12:51 (bottom) UT on May 19, 2007. Right: corresponding prominence altitude maps. A comparison between the top right and bottom right panels shows the increase in the prominence altitude in 10 min of time interval (adapted from Gissot et al., 2008).

stereoscopy developed within the Solar Software library[1] and in particular of the scc_measure.pro routine. This routine (developed by Thompson and applied by the developer to reconstruct the 3D orientation of sungrazing comet tails; see Thompson, 2009) after reading in a pair of STEREO EUVI A and B images, is able to trace the LOS of a point selected in one image pair into the field-of-view of the second image, and then provides the 3D coordinates (altitude, latitude and longitude) of the selected point.

An example of results obtained with this technique is shown in Fig. 7 for a filament (top, from Liewer et al., 2009) and a prominence (bottom, from Bemporad, 2009). In particular, Liewer et al. (2009) studied with the "tie-pointing" technique the same eruptive filament previously studied by Gissot et al. (2008) with their "optical flow" algorithm. Results found with the two techniques are in good agreement (altitude of $\sim$44 Mm), if the position of the highest point as derived by Liewer et al. (2009) is considered. Liewer et al. (2009) concluded that the EUV filament (as observed by STEREO) is located at higher altitude with respect to the Hα filament (observed by the Kanzelöhe Solar Observatory), thus in agreement with results previously derived by Schwartz et al. (2004) from their spectroscopic model of the filament. Moreover, in this work the authors concluded that the filament starts to be activated (i.e. heated) before the final flare, but the rapid rise of the filament from a height of 1–2 solar radii immediately follows the flare peak. Interestingly, by also taking advantage of Hα observations, the authors demonstrated from their analysis that the post-flare ribbons and loops were located directly beneath the former location of the filament, as envisaged in the unified solar eruption model (see Forbes, 2000).

The first 3D reconstruction with "tie-pointing" technique of an erupting prominence (i.e. observed off-limb) has been performed in Bemporad (2009) (Fig. 7, bottom panels). In this work it was shown that (similarly to the event reported by Gissot et al., 2008; Liewer et al., 2009) the prominence erupted asymmetrically. During its expansion the prominence assumed the shape of a "hook" with its base (corresponding to one of the two prominence footpoints) anchored at the Sun; no flares are observed during this event. The 3D reconstruction shows that the prominence can be approximated mainly as a 2D ribbon-like feature and that $\sim$12 min after the rising start time the distribution of the erupting material is nearly planar; this is in agreement with the usual ribbon-like appearance of filaments in Hα. Interestingly, from the analysis of STEREO data it is found that the 2D distribution of plasma is mainly "preserved" during the eruption. In fact, the high spatial resolution ($\sim$1.5 in pixel^{-1}) of EUVI He II λ304 images and the very high temporal cadence of these observations ($\sim$37 s frame^{-1}), enabled the tracking of well identified He II features during the eruption and to reconstruct their trajectory. It was found for the first time that the prominence expands anisotropically, because the expansion rate in the direction perpendicular to the prominence plane was $\sim$10 times smaller than the expansion rate observed in the direction parallel to that plane. This phenomenon, yet to be explained, is likely to be related to the unknown 3D configuration of the magnetic field supporting the prominence plasma and driving the eruption. The "tie-pointing" technique has also been recently applied by Li et al. (2010), who found clear signatures of **anisotropic** expansion of two erupting filaments from their 3D reconstruction, in agreement with previous results by Bemporad (2009). In particular, the authors conclude that the velocity and acceleration vary with the measured location within the erupting features and that the two filaments originate from the same filament channel.

As also noticed by Bemporad (2009) and Liewer et al. (2009), the "tie-pointing" technique can be successfully applied only for small separation angles between the two spacecrafts, when the correct

[1] Freely distributed on the web at http://sohowww.nascom.nasa.gov/solarsoft/.

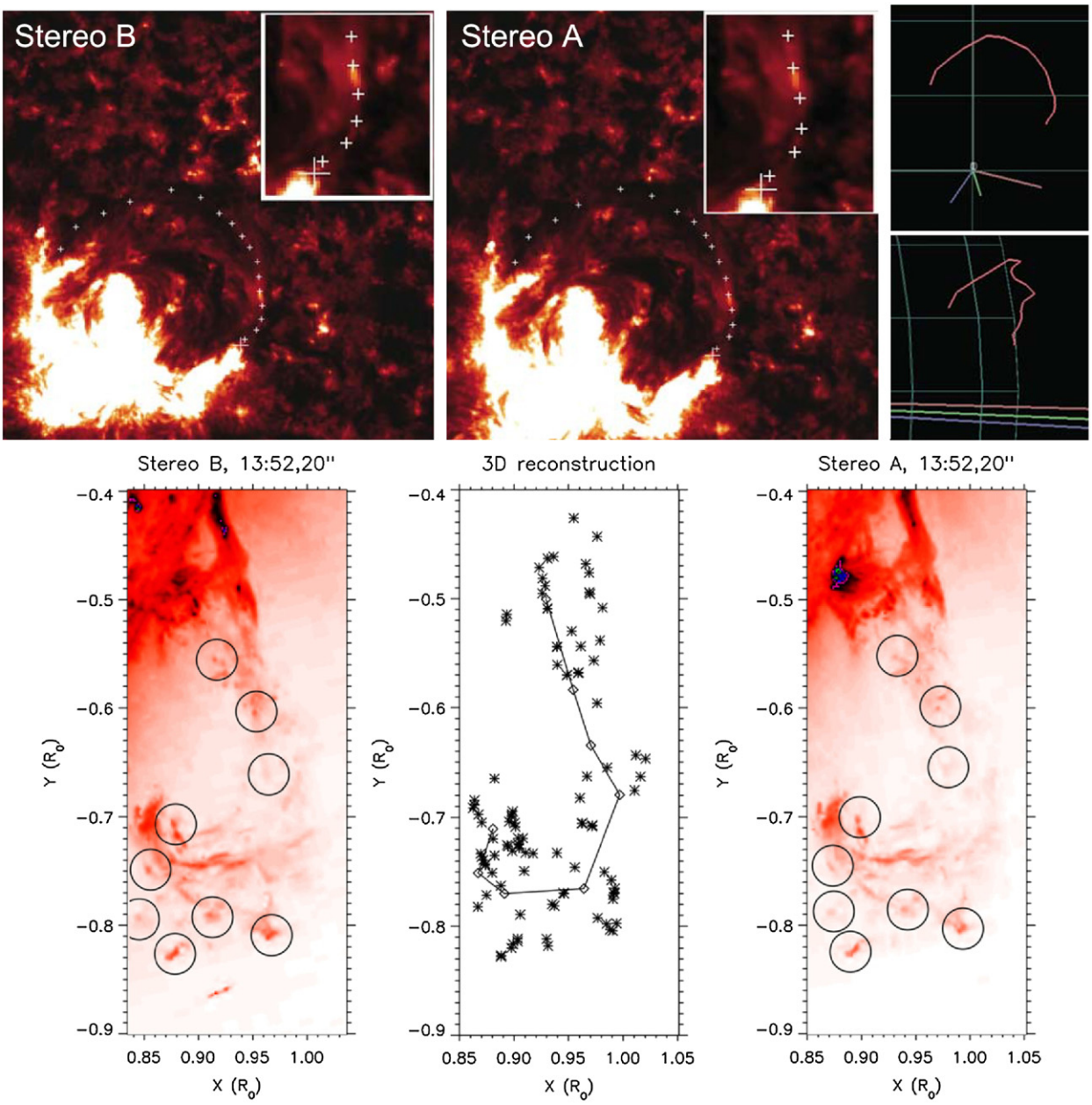

Fig. 7. Examples of applications of "tie-pointing" technique for 3D reconstruction of an erupting filament (top) and a prominence (bottom), both observed in the He II λ304 line. Top: example of pair points selected along a filament in the STEREO-B (left) and -A (middle) images and the resulting 3D filament structure (right) (adapted from Liewer et al., 2009). Bottom: example of pair points selected along a prominence in the STEREO-B (left) and -A (right) images and the resulting 3D prominence structure (middle) (adapted from Bemporad, 2009).

"pair association" (i.e. identification of the *same* feature in both images) is possible, while for larger angles of separation these methods present larger difficulties in identifying common features. In any case, important information on the 3D structure of filaments can be derived even in the case of large separation angle, as it has been demonstrated by Gosain et al. (2009) and Gosain and Schmieder (2010). In these works the authors studied a filament which erupted on May 22, 2008 (when the separation angle between the STEREO spacecraft was 52.4°) and showed that the inclination of the filament with respect to the Sun surface can be derived with two different techniques. Gosain et al. (2009) used mainly the "tie-pointing" technique: the position of one of the filament feet *F* and of a filament point *P* located at the same latitude as *F* have been determined by "tie-pointing". It turns out that the segment *P*–*F* is not perpendicular to the Sun surface and that the filament has an inclination angle of 43°. In Gosain and Schmieder (2010) the authors developed a different technique which allows at the same time the determination of the filament width and its inclination with respect to the solar surface. By assuming that the filament can be approximated as an infinitely thin 2D planar plasma sheet anchored at the Sun, changes in the projected filament width when observed at the same time from two different view points can be entirely ascribed to its inclination with respect to the solar surface (see Gosain and Schmieder, 2010, for details). By applying this technique to the same filament studied by Gosain et al. (2009), the authors derived an inclination angle of 54°, in fairly good agreement with their previous estimate (43°) derived with "tie-pointing" technique.

A limit to the 3D reconstruction of erupting filaments is provided by the fact that some filaments (before their "activation")

are seen in the He II λ304 band in absorption as dark structures on the disk and in emission as prominences above the limb. Hence, as an eruption occurs, filaments become diffuse and lose very quickly their contrast with respect to the background surface features, becoming hardly detectable. Very recently, an interesting technique for improving this contrast by taking advantage of the two STEREO-A and -B views has been developed by Artzner et al. (2010). The authors showed that it is possible in general to apply a geometric transformation which projects the image seen from the first spacecraft (for example, STEREO-B) into the field-of-view of the second one (STEREO-A). Then, when a filament is observed on disk from both spacecrafts at the same time, the difference between the STEREO-A and the projected STEREO-B images enhances the visibility of the filament, which appears as a "black and white couple", while background features are completely removed (see Fig. 8). This happens because the filament (1) is an elevated structure not lying on the same spherical surface as the background features (plages and network), appearing different in the transformed view, and (2) is a 3D structure while other background features can be approximated as 2D features. In particular, the authors applied this technique to the STEREO sequence of the same filament eruption studied by Gosain et al. (2009) and Gosain and Schmieder (2010), when the separation angle between the spacecraft was 52.4°: processed images show very well the erupting filament, otherwise hardly identifiable in pre-processed images.

An interesting technique to derive information on the 3D distribution of prominence plasma has been developed by Väsquez et al. (2009). Before the STEREO mission, it has been demonstrated that a series of images made of the corona over a solar rotation show a steadily changing appearance; by assuming that this variation is solely due to the rotation of a static corona, a 3D reconstruction of coronal densities may be built: this is the approach of solar rotational tomography (SRT) (see Frazin, 2000, for a description of this technique). Väsquez et al. (2009) applied the differential emission measure tomography technique (theoretically described by Frazin et al., 2005) to demonstrate that the 3D distribution not only of coronal density, but also of temperature can be reconstructed via the 3D tomographic analysis of EUV images acquired with three different Fe filters. The use of STEREO images acquired from two different points of view allowed the authors to reduce the time required to have information over a full coronal rotation, thus making the hypothesis of a "frozen corona" less stringent. Interestingly, Väsquez et al. (2009) showed that this technique can be used to derive not only global information on the whole corona, but also on specific structures such as prominence cavities (which are apparently different from EUV filaments; see, e.g. Heinzel et al., 2008). From the 3D reconstruction the authors demonstrate that polar crown filaments (mapped in He II images) are located in regions of reduced emission in the 171, 195 and 284 Å bands, where the electron density is locally lower (see Fig. 9). These filament-cavities are ubiquitously observed at the base of helmet streamers and have direct analog in the observed three-part structure of many CMEs. Filament-cavities studied by Väsquez et al. (2009), not clearly discernible above the limb in EUV images, are located at lower altitudes with respect to coronal streamer cavities, becoming unobservable in white light coronagraphs; thus 3D tomography is the only option to study their plasma properties quantitatively.

Very recently, an important information on the "roll effect" in erupting prominences has been derived from STEREO EUVI data by Panasenco et al. (this issue), who found evidence of sideways rolling motions of erupting prominences. The authors interpreted this effect as a consequence of force imbalance inside the filament arcade related to the adjacent large coronal holes, while the observed non-radial motions of the resulting CME are interpreted as a signature of global magnetic configuration force imbalance. Moreover, the occurrence of strong rotation of an erupting quiescent polar crown prominence, in agreement with the idea of untwisting of a helical flux rope, has been recently reported from STEREO data by Thompson (this issue) for an event which occurred on June 6, 2007 (see Thompson, this issue).

6. Discussion and conclusions

Thanks to the STEREO mission it is now possible to derive with few assumptions information on the 3D plasma distribution within solar prominences and filaments. One can also infer their full 3D kinematical parameters (velocity and acceleration vectors) when these structures erupt. These information, coupled with additional plasma physical parameters as derived by other ground- and space-based observatories, have in principle the potential to help us find a final solution to many open problems on the formation, stability and eruption of solar prominences. Nevertheless, as shown in the present review, the full potential of STEREO data in solving these problems has not been utilized so far. This conclusion is supported by the following two remarks.

First, a comparison of results on the 3D structure and kinematic of prominences/filaments as derived with STEREO data (Section 5) with results derived with data available before STEREO (Section 4) shows that little advancement has been achieved. In particular, filament altitude maps similar to those derived by Gissot et al. (2008) with STEREO data were also derived by Schwartz et al. (2004), hence prior to STEREO, even if the spectroscopic model developed by Schwartz et al. (2004) requires much stronger

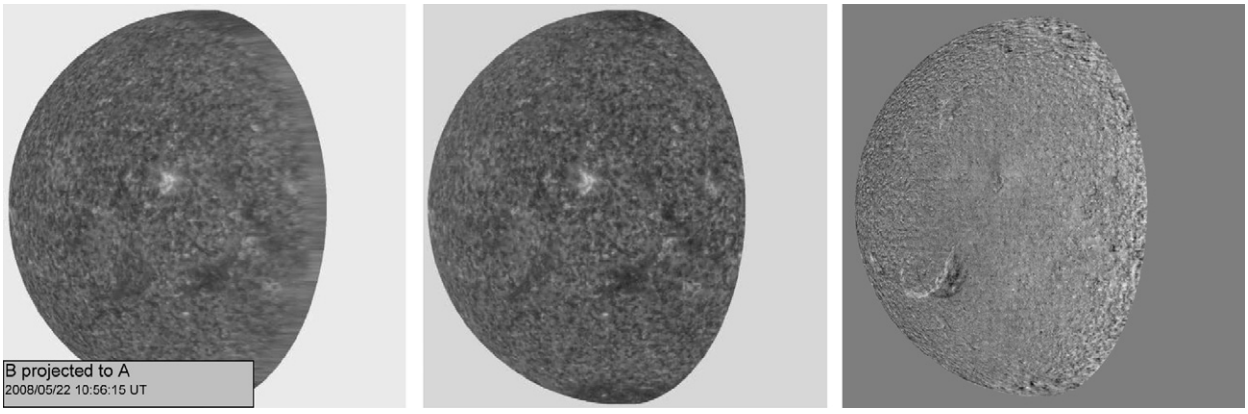

Fig. 8. An example of He II λ304 chromospheric background removal by taking advantage of STEREO EUVI images. With this technique the image observed by STEREO-B has been rotated and projected in the field of view of STEREO-A (left); by subtracting the projected STEREO-B image from the STEREO-A image (middle) the filament is enhanced as a "black and white couple" in the difference image (right; adapted from Artzner et al., 2010).

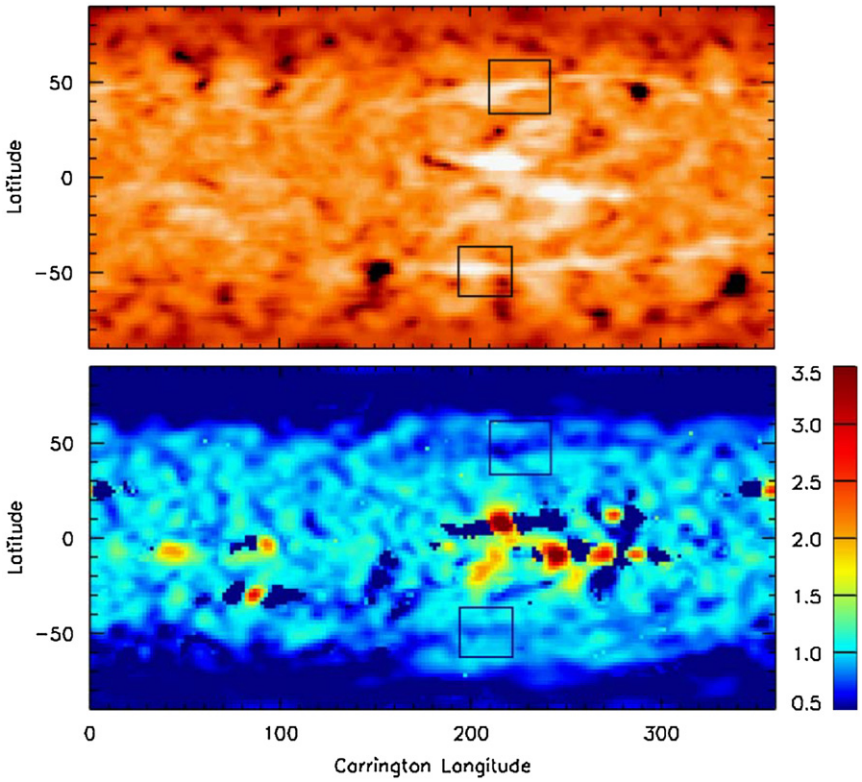

Fig. 9. Carrington rotation map of tomographic 3D reconstruction of the He II emission (top) and corresponding electron density (bottom); the comparison between the two maps shows that polar crown filaments are located in correspondence of underlying low density regions (cavities; adapted from Väsquez et al., 2009).

assumptions on unknown quantities with respect to the Gissot et al. (2008) analysis. Also, 3D trajectories of prominences similar to those derived by Bemporad (2009) and Liewer et al. (2009) with the "tie-pointing" technique applied to STEREO data are mainly analogous to trajectories inferred by Zapiör and Rudawy (2007) by combining Hα images and spectra.

Secondly, as also admitted by Liewer et al. (2009) referring in their particular study, "the stereoscopic analysis has not shed light on the underlying cause of the eruption"; the same conclusion holds mainly for all others works described above dealing with STEREO observations of filaments/prominences. For instance, Gissot et al. (2008) concluded that "the flare starts after the onset of the filament eruption", while from the analysis of the same filament eruption Liewer et al. (2009) found a slow rise starting ~6 h before the flare (not observed by Gissot et al., 2008) and concluded that "the rapid rise from one to two solar radii immediately follows the flare peak". Hence, from these two works it is not possible, for instance, to solve the decades-old controversy viz. whether the flare (i.e. magnetic reconnection) causes the eruption or vice-versa (see for recent results on this open issue Sterling et al., 2007). Also, no information has been derived so far from STEREO data on the open problems of prominence formation, accretion and stability.

These limitations can be explained at least by the following two reasons. First, STEREO was launched during the long duration Solar Cycle minimum (October 2006) and with time, because of the increasing angle of separation between the two STEREO spacecrafts, it increasingly became difficult in the following years to reconstruct the structures in 3D. Hence, a very small number of active region filaments/prominences (those better visible in the He II λ304 filter) were available so far for 3D reconstructions. Secondly, as a matter of fact all the 3D reconstructions performed so far concerns only filaments/prominences observed by STEREO during their activation phase and subsequently their eruptive phase. This can be related to differences between the He II λ304 filters onboard STEREO with respect to those employed for the SOHO/EIT instrument, resulting in a better imaging of filaments with STEREO only when they activate. Because the important forces for supporting stable filaments are completely different from those working in erupting prominences, observations concerning only erupting prominences obviously cannot tell us "the whole story" about the problem of prominence stability and destabilization.

In any case, it is important to emphasize that analyses conducted so far with STEREO gave us the opportunity to confirm much of what was learned from previous techniques described above for deducing the overall configurations of filaments, even though these analyses to date have not yet shown anything about the pre-eruptive configurations that is truly new. Hence, major efforts are needed in the near future in order to extract all the information potentially concealed in the STEREO observations of prominences and to combine observational results with theoretical modelling. For instance, it will be necessary to develop new data reduction techniques aimed at deriving physical quantities in prominence plasma (e.g. the optical thickness) taking into account that STEREO-A and -B do not integrate the same structures along the LOS. To this end, observations from both ground-based solar observatories and all other space-based observatories located at the Lagrangian point L1 (e.g. SOHO) or in Sun-synchronous orbit around the Earth (e.g. TRACE, Hinode, SDO) will provide a fundamental third viewing perspective combined with the two different views from STEREO. Moreover, it will also be necessary to combine stereoscopic observations with measurements of unknown chromospheric and coronal magnetic field, which is at present considered something as a "dark energy" by solar physicists, because "we know it permeates the corona and controls its static and dynamic behavior, yet we are unable to usefully measure it" (Lin et al., 2004). For

instance, very interesting results have been recently derived by Aschwanden and Sandman (2010) from the observed misalignment between the 3D reconstructions of coronal loops from STEREO data and the extrapolated magnetic fieldlines. Hence, the combination of spectro-polarimetric measurements of the coronal magnetic fields responsible for the prominences/filaments equilibrium with 3D stereoscopic reconstructions will likely give us the final answers to many of the still open questions on these phenomena.

Acknowledgments

The author acknowledges support from ASI/INAF I/023/09/0 Contract. Very useful comments and suggestions from the anonymous referees are gratefully acknowledged. *STEREO* is a NASA mission.

References

Antonucci, E., Kohl, J.L., Noci, G., et al., 1997. Velocity fields in the solar corona during mass ejections as observed with UVCS-SOHO. Astrophys. J. 490, L183–L186.
Artzner, G., Gosain, S., Schmieder, B., 2010. A technique for removing background features in SECCHI–EUVI He II 304 A filtergrams: application to the filament eruption of 22 May 2008, arXiv:1001.4884.
Aschwanden, M.J., Bastian, T.S., 1994. VLA stereoscopy of solar active regions. 1: method and tests. Astrophys. J. 426, 425–433.
Aschwanden, M.J., Lim, J., Gary, D.E., Klimchuk, J.A., 1995. Solar rotation stereoscopy in microwaves. Astrophys. J. 454, 512–521.
Aschwanden, M.J., Sandman, A.W., 2010. Bootstrapping the coronal magnetic field with STEREO: unipolar potential field modeling. Astrophys. J. 140, 723–734.
Athay, R.G., Querfeld, C.W., Smartt, R.N., et al., 1983. Vector magnetic fields in prominences. III—HeI D3 Stokes profile analysis for quiescent and eruptive prominences. Sol. Phys. 89, 3–30.
Bemporad, A., Del Zanna, G., Andretta, V., Poletto, G., 2009. Multispacecraft observations of a prominence eruption. Ann. Geophys. 27 (10), 3841–3851.
Bemporad, A., 2009. Stereoscopic reconstruction from STEREO/EUV imagers data of the three-dimensional shape and expansion of an erupting prominence. Astrophys. J. 701, 298–305.
Berger, M.A., Field, G.B., 1984. The topological properties of magnetic helicity. J. Fluid Mech. 147, 133–148.
Brajša, R., Romštajn, I., Wöhl, H., et al., 2009. Heights of solar tracers observed at 8 mm and an interpretation of their radiation. Astron. Astrophys. 493, 613–621.
Ciaravella, A., Raymond, J.C., Thompson, B.J., et al., 2000. Solar and heliospheric observatory observations of a helical coronal mass ejection. Astrophys. J. 529, 575–591.
Ciaravella, A., Raymond, J.C., van Ballegooijen, A., et al., 2003. Physical parameters of the 2000 February 11 coronal mass ejection: ultraviolet spectra versus white-light images. Astrophys. J. 597, 1118–1134.
Curdt, W., Wilhelm, K., Feng, L., Kamio, S., 2008. Multi-spacecraft observations of polar coronal plumes. Astron. Astrophys. 481, L61–L64.
Feng, L., Inhester, B., Solanki, S., et al., 2007. First stereoscopic coronal loop reconstructions from STEREO SECCHI images. Astrophys. J. 671, L205–L208.
Filippov, B.P., Den, O.G., 2001. A critical height of quiescent prominences before eruption. J. Geophys. Res. 106 (A11), 25177–25184.
Forbes, T., 2000. A review on the genesis of coronal mass ejections. J. Geophys. Res. 105 (A10), 23153–23166.
Frazin, R.A., 2000. Tomography of the solar corona. I. A robust, regularized, positive estimation method. Astrophys. J. 530, 1026–1035.
Frazin, R.A., Kamalabadi, F., Weber, M.A., 2005. On the combination of differential emission measure analysis and rotational tomography for three-dimensional solar EUV imaging. Astrophys. J. 628, 1070–1080.
Gissot, S.F., Hochedez, J.-F., Dibos, F., et al., 2003. Extracting the apparent motion from two successive EIT images. In: Wilson, A. (Ed.), Proceedings of Solar Variability as an Input to the Earth's Environment Meeting, ESA SP-535, Noordwijk, pp. 853–856.
Gissot, S.F., Hochedez, J.-F., 2007. Multiscale optical flow probing of dynamics in solar EUV images. Algorithm, calibration, and first results. Astron. Astrophys. 464, 1107–1118.
Gissot, S.F., Hochedez, J.-F., Chainais, P., Antoine, J.-P., 2008. 3D reconstruction from SECCHI-EUVI images using an optical-flow algorithm: method description and observation of an erupting filament. Sol. Phys. 252, 397–408.
Gosain, S., Schmieder, B., Venkatakrishnan, P., et al., 2009. 3D evolution of a filament disappearance event observed by STEREO. Sol. Phys. 259, 13–30.
Gosain, S., Schmieder, B., 2010. Estimation of width and inclination of a filament sheet using He II 304 Å observations by STEREO/EUVI. Ann. Geophys. 28, 149–153.
Green, L.M., Kliem, B., Török, T., van Driel-Gesztelyi, L., Attrill, G.D.R., 2007. Transient coronal sigmoids and rotating erupting flux ropes. Sol. Phys. 246, 365–391.
Heinzel, P., Schmieder, B., Tziotziou, K., 2001. Why are solar filaments more extended in extreme-ultraviolet lines than in Hα. Astrophys. J. 561, L223–L227.
Heinzel, P., Anzer, U., Schmieder, B., 2003. A spectroscopic model of euv filaments. Sol. Phys. 216, 159–171.
Heinzel, P., Schmieder, B., Fárník, F., et al., 2008. Hinode, TRACE, SOHO, and ground-based observations of a quiescent prominence. Astrophys. J. 686, 1383–1396.
Hood, A.W., Priest, E.R., 1981. Critical conditions for magnetic instabilities in force-free coronal loops. Geophys. Astrophys. Fluid Dyn. 17, 297–318.
Howard, R.A., Moses, J.D., Vourlidas, A., et al., 2008. Sun Earth connection coronal and heliospheric investigation (SECCHI). Space Sci. Rev. 136, 67–115.
Inhester, B., 2006. Stereoscopy basics for the STEREO mission, arXiv:astro-ph/0612649.
Joshi, V., Srivastava, N., 2007. On the study of kinematics of eruptive quiescent prominences observed in He 304 Å. Bull. Astron. Soc. India 35, 447–455.
Kaiser, M.L., Kucera, T.A., Davila, J.M., et al., 2008. The STEREO mission: an introduction. Space Sci. Rev. 136, 5–16.
Kohl, J.L., Noci, G., Cranmer, S.R., Raymond, J.C., 2006. Ultraviolet spectroscopy of the extended solar corona. Astron. Astrophys. Rev. 13, 31–157.
Labrosse, N., Gouttebroze, P., 2001. Formation of helium spectrum in solar quiescent prominences. Astron. Astrophys. 380, 323–340.
Labrosse, N., Gouttebroze, P., Vial, J.-C., 2007. Effect of motions in prominences on the helium resonance lines in the extreme ultraviolet. Astron. Astrophys. 463, 1171–1179.
Labrosse, N., Heinzel, P., Vial, J.-C., et al., 2010. Physics of solar prominences: I. Spectral diagnostics and non-LTE modelling. Space Sci. Rev. 151, 243–332.
Landi, E., Raymond, J.C., Miralles, M.P., Hara, H., 2010. Physical conditions in a coronal mass ejection from Hinode, Stereo, and SOHO observations. Astrophys. J. 711 (1), 75–98.
Li, T., Zhang, J., Zhao, H., Yang, S., 2010. Three-dimensional shape and evolution of two eruptive filaments. Astrophys. J. 720, 144–149.
Liewer, P.C., De Jong, E.M., Hall, J.R., et al., 2009. Stereoscopic analysis of the 19 May 2007 erupting filament. Sol. Phys. 256, 57–72.
Lin, H., Kuhn, J.R., Coulter, R., 2004. Coronal magnetic field measurements. Astrophys. J. 613, L177–L180.
Low, B.C., Fong, B., Fan, Y., 2003. The mass of a solar quiescent prominence. Astrophys. J. 594, 1060–1067.
Mackay, D.H., Karpen, J.T., Ballester, J.L., et al., 2010. Physics of solar prominences: II. Magnetic structure and dynamics. Space Sci. Rev. 151, 333–399.
Martin, S.F., Ramsey, H.E., Carroll, G.A., Martin, D.C., 1974. A multi-slit spectrograph and Hα Doppler system. Sol. Phys. 37, 343–350.
Martin, S.F., 1998. Conditions for the formation and maintenance of filaments. Sol. Phys. 182, 107–137.
Martin, S.F., 2003. Signs of helicity in solar prominences and related features. Adv. Space Res. 32, 1883–1893.
McMath, R.R., Pettit, E., 1939. The Doppler effect in an eruptive prominence. Publ. Astron. Soc. Pac. 51, 154.
Mein, P., Mein, N., 1991. Dynamical fine structure of a quiescent prominence. Sol. Phys. 136, 317–333.
Mierla, M., Inhester, B., Marqué, C., et al., 2009. On 3D reconstruction of coronal mass ejections: I. Method description and application to SECCHI-COR data. Sol. Phys. 259, 123–141.
Noci, G., Kohl, J.L., Withbroe, G.L., 1987. Solar wind diagnostics from Doppler-enhanced scattering. Astrophys. J. 315, 706–715.
Panasenco, O., Martin, S., Joshi, A.D., Srivastava, N., this issue. Rolling motion in erupting prominences observed by STEREO. J. Atmos. Solar-Terr. Phys., doi:10.1016/j.jastp.2010.09.010.
Patsourakos, S., Vial, J.-C., 2002. Soho contribution to prominence science. Sol. Phys. 208, 253–281.
Ricca, R.L., 1994. Writhe and twist helicity contributions to a magnetic flux loop and hammock configuration. In: Belvedere, G., Rodonó, M., Schmieder, B., Simnett, G.M. (Eds.), Poster Papers Presented at the "Seventh European Meeting on Solar Physics", 11–15 May 1993, Catania, Italy, Catania Astrophysical Observatory Special Publication, p. 151.
Roša, D., Vršnak, B., Božić, H., et al., 1998. A method to determine the solar synodic rotation rate and the height of tracers. Sol. Phys. 179, 237–252.
Rudawy, P., Cader-Sroka, B., Rompolt, B., et al., 2003. 3D evolution of an eruptive prominence of 15 May 2000 and the associated active phenomena. In: Wilson, A. (Ed.), Proceedings of the Solar Variability as an Input to the Earth's Environment Meeting ESA SP-535, Noordwijk, pp. 507–509.
Rust, D.M., Kumar, A., 1984. Helical magnetic fields in filaments. Sol. Phys. 155, 69–97.
Schmieder, B., Lin, Y., Heinzel, P., Schwartz, P., 2004. Multi wavelength study of a high latitude EUV filament. Sol. Phys. 221, 297–323.
Schmieder, B., Chandra, R., Berlicki, A., Mein, P., 2010. Velocity vectors of a quiescent prominence observed by Hinode/SOT and the MSDP (Meudon). Astron. Astrophys. 514, A68.
Schwartz, P., Heinzel, P., Anzer, U., Schmieder, B., 2004. Determination of the 3D structure of an EUV-filament observed by SoHO/CDS, SoHO/SUMER and VTT/MSDP. Astron. Astrophys. 421, 323–338.
Schwartz, P., Heinzel, P., Schmieder, B., Anzer, U., 2006. Study of an extended EUV filament using SoHO/SUMER observations of the hydrogen Lyman lines. Astron. Astrophys. 459, 651–661.
Srivastava, N., Mathew, S.-K., 1999. A digital imaging multi-slit spectrograph for measurement of line-of-sight velocities on the sun. Sol. Phys. 185, 61–68.
Sterling, A., Harra, L.K., Moore, R.L., 2007. New evidence for the role of emerging flux in a solar filament's slow rise preceding its CME-producing fast eruption. Astrophys. J. 669 (2), 1359–1371.

Suleiman, R.M., Crooker, N.U., Raymond, J.C., van Ballegooijen, A., 2005. UVCS observations of a helical CME structure. In: Coronal, Stellar Mass Ejections, IAU Symposium 226, Cambridge University Press, Cambridge, pp. 71–75.
Thompson, W.T., 2006. Coordinate systems for solar image data. Astron. Astrophys. 449 (2), 791–803.
Thompson, W.T., 2009. 3D triangulation of a sun-grazing comet. Icarus 200 (2), 351–357.
Thompson, W.T., this issue. Strong rotation of an erupting quiescent polar crown prominence. J. Atmos. Solar-Terr. Phys., doi:10.1016/j.jastp.2010.07.005.
Tonooka, H., Matsumoto, R., Miyaji, S., et al., 2000. Simultaneous Hα and X-ray observations of prominence eruption and disappearance. Adv. Space Res. 26 (3), 473–476.
Török, T., Kliem, B., 2005. Confined and ejective eruptions of kink-unstable flux ropes. Astrophys. J. 630, L97–L100.
Väsquez, A.M., Frazin, R.A., Kamalabadi, F., 2009. 3D temperatures and densities of the solar corona via multi-spacecraft EUV: tomography: analysis of prominence cavities. Sol. Phys. 256, 73–85.
Vourlidas, A., Thernisien, A., this issue. CME reconstruction: pre-STEREO and STEREO era. J. Atmos. Solar-Terr. Phys., doi:10.1016/j.jastp.2010.10.019.
Vršnak, B., Roša, D., Božič, H., 1999. Height of tracers and the correction of the measured solar synodic rotation rate: demonstration of the method. Sol. Phys. 185, 207–225.
Wimmer-Schweingruber, R.F., 2006. Coronal mass ejections. Space Sci. Rev. 123, 471–480.
Wuelser, J.-P., Lemen, J.R., Tarbell, T.D., et al., 2004. EUVI the STEREO-SECCHI extreme ultraviolet imager. In: Fineschi, S., Gummin, M.A. (Eds.), Proceedings of the SPIE, vol. 5171, pp. 111–122.
Yurchyshyn, V.B., Wang, H., Goode, P.R., Deng, Y., 2001. Orientation of the magnetic fields in interplanetary flux ropes and solar filaments. Astrophys. J. 563, 381–388.
Yurchyshyn, V., Yashiro, S., Abramenko, V., Wang, H., Gopalswamy, N., 2005. Statistical distributions of speeds of coronal mass ejections. Astrophys. J. 619, 599–603.
Zapiör, M., Rudawy, P., 2007. Determination of true 3D trajectories of solar prominences' blobs. Cent. Eur. Astrophys. Bull. 31, 287–296.
Zhou, G.P., Wang, J.X., Zhang, J., et al., 2006. Two successive coronal mass ejections driven by the kink and drainage instabilities of an eruptive prominence. Astrophys. J. 651, 1238–1244.
Zurbuchen, T.H., Richardson, I.G., 2006. In situ solar wind and magnetic field signatures of interplanetary coronal mass ejections. Space Sci. Rev. 123, 31–43.